6th European Conference on Computational Mechanics (ECCM 6)
7th European Conference on Computational Fluid Dynamics (ECFD 7)
1115 June 2018, Glasgow, UK

EFFICIENT INTEGRATION FOR THE SIMO-MIEHE MODEL WITH MOONEY-RIVLIN POTENTIAL

ALEXEY V. SHUTOV[12]

[1] Lavrentyev Institute of Hydrodynamics
Lavrentyeva 15, Novosibirsk, 630090, Russia
alexey.v.shutov@gmail.com www.hydro.nsc.ru

[2] Novosibirsk State University
Pirogova 1, Novosibirsk, 630090, Russia
alexey.v.shutov@gmail.com www.nsu.ru

Key words: Finite Strain, Simo-Miehe Model, Mooney-Rivlin Potential, Efficient Numerics, Zener Model, Stress-Dependent Viscosity

Abstract. A model of finite-strain visco-plasticity proposed by Simo and Miehe (1992) is considered. The model is based on the multiplicative split of the deformation gradient, combined with hyperelastic relations between elastic strains and stresses. This setup is a backbone of many advanced models of visco-elasticity and visco-plasticity. Therefore, its efficient numerical treatment is of practical interest. Since the underlying evolution equation is stiff, implicit time integration is required. A discretization of Euler backward type yields a system of nonlinear algebraic equations. The system is usually solved numerically by Newton-Raphson iteration or its modifications. In the current study, a practically important case of the Mooney-Rivlin potential is analyzed. The solution of the discretized evolution equation can be obtained in a closed form in case of a constant viscosity. In a more general case of stress-dependent viscosity, the problem is reduced to the solution of a single scalar equation or, in some situations, even can be solved explicitly. Simulation results for demonstration problems pertaining to large-strain deformation of different types of viscoelastic materials are presented.

1 INTRODUCTION

The Simo and Miehe version of the Maxwell fluid was initially presented in [1] as a part of a more general viscoplastic material model. The main ingredients of this formulation are the multiplicative decomposition of the deformation gradient and hyperelastic relations between stresses and elastic strains. A Lagrangian formulation of this model was considered later in [2]. As shown in [3], the approach of Simo and Miehe has numerous advantages over alternative formulations proposed for the Maxwell fluid. Due to its superior properties, it was advocated in the fundamental work on finite-strain viscoelasticity [4]. Interestingly, in the course of subsequent years, the Simo and Miehe version of the Maxwell fluid war rediscovered by other authors (cf. the discussion in [5]).

Dealing with a single Maxwell element, the corresponding evolution equations are six dimensional. In real computations, the time step size can become larger than the typical relaxation time of this element. Therefore, implicit integration of the underlying evolution equation is needed. The time discretization yields a system of six nonlinear algebraic equations with respect to six unknown components of the tensor-valued internal variable. The spectral decomposition allows one to reduce the problem to finding three eigenvalues [6, 4]. In any case, the obtained nonlinear systems of equations are solved by an iterative Newton-Raphson-like procedure [4, 7, 8, 9, 10, 11, 12, 13, 14]. Unfortunately, iteration-based procedures may suffer from a lack of robustness and poor computational efficiency. Problem-adapted algorithms based on a closed-form solution of the underlying system of equations are more preferable.

Such problem-adapted algorithms can be constructed by exploiting the form of the strain energy function. For instance, an explicit update formula was obtained for the classical neo-Hookean potential in [15]. A simple generalization of this numerical scheme to the strain energy of Yeoh type was presented in [16]. An extension to the thermo-mechanical case was presented in [17, 18]. Hybrid explicit/implicit procedures can be obtained for viscoplasticity with nonlinear kinematic hardening. Indeed, the explicit update formula for the Maxwell fluid allows us to build a scheme which is more stable than a purely explicit one (cf. [19, 20]). Moreover, the closed-form solution reported in [15] is implemented as a part of a more general numerical procedures for finite-strain viscoplasticity (cf. [21]) and finite strain creep (cf. [22]). In [23] the explicit update formula was implemented to model the large-strain viscoelastic behavior of a bituminous binding agent.

The main goal of the current study is to analyze the applicability of the refined efficient numerical algorithms to the case of stress-dependent viscosity. Previously proposed methods are briefly summarized and new modifications are considered. Just as the original counterparts proposed for constant viscosity, the new methods are unconditionally stable. They exactly preserves the incompressibility of the inelastic flow and weak invariance under isochoric changes of the reference configuration (for a general definition of the weak invariance, the reader is referred to [24]).

2 BASIC MATERIAL MODEL: MAXWELL FLUID WITH A CONSTANT VISCOSITY

2.1 Lagrangian formulation

Let us briefly recall the version of the Maxwell fluid, proposed by Simo and Miehe in [1]. In this subsection we focus on its Lagrangian formulation (cf. [2]). By $\mathbf{F}$ denote the deformation gradient tensor. It is decomposed into the inelastic part $\mathbf{F}_{\mathrm{i}}$ and the elastic part $\hat{\mathbf{F}}_{\mathrm{e}}$

$$\mathbf{F} = \hat{\mathbf{F}}_{\mathrm{e}}\mathbf{F}_{\mathrm{i}}. \tag{1}$$

To filter out superimposed rigid body rotations, the following tensors of the right Cauchy-Green type are introduced

$$\mathbf{C} := \mathbf{F}^{\mathrm{T}}\mathbf{F}, \quad \mathbf{C}_{\mathrm{i}} := \mathbf{F}_{\mathrm{i}}^{\mathrm{T}}\mathbf{F}_{\mathrm{i}}. \tag{2}$$

Let ψ be the Helmholz free energy per unit mass. We assume that ψ is an isotropic function of the tensor argument $\mathbf{C}\mathbf{C}_{\mathrm{i}}^{-1}$. For the the Mooney-Rivlin potential we have

$$\rho_{\mathrm{R}}\psi = \frac{c_{10}}{2}\big(\mathrm{tr}\overline{\mathbf{C}\mathbf{C}_{\mathrm{i}}^{-1}} - 3\big) + \frac{c_{01}}{2}\big(\mathrm{tr}\overline{(\mathbf{C}\mathbf{C}_{\mathrm{i}}^{-1})^{-1}} - 3\big), \tag{3}$$

where ρ_R is the mass density of the material in the reference configuration; the overline stands for the unimodular part: $\overline{\mathbf{A}} := (\det\mathbf{A})^{-1/3}\mathbf{A}$; c_{10} and c_{01} are fixed material constants. The neo-Hookean potential is restored for $c_{01} = 0$. The second Piola-Kirchhoff stress $\tilde{\mathbf{T}}$ is computed as

$$\tilde{\mathbf{T}} = 2\rho_{\mathrm{R}}\frac{\partial\psi(\mathbf{C}\mathbf{C}_{\mathrm{i}}{}^{-1})}{\partial\mathbf{C}}\Big|_{\mathbf{C}_{\mathrm{i}}=\mathrm{const}} = \mathbf{C}^{-1}(c_{10}\overline{\mathbf{C}}\mathbf{C}_{\mathrm{i}}^{-1} - c_{01}\mathbf{C}_{\mathrm{i}}\overline{\mathbf{C}^{-1}})^{\mathrm{D}}. \tag{4}$$

Here, $\mathbf{A}^{\mathrm{D}} := \mathbf{A} - \frac{1}{3}(\mathrm{tr}\mathbf{A})\mathbf{1}$. The evolution of the inelastic strain is governed by the ordinary differential equation with initial condition

$$\dot{\mathbf{C}}_{\mathrm{i}} = \frac{1}{\eta}\big(\mathbf{C}\tilde{\mathbf{T}}\big)^{\mathrm{D}}\mathbf{C}_{\mathrm{i}} = \frac{1}{\eta}\big(c_{10}\overline{\mathbf{C}}\mathbf{C}_{\mathrm{i}}^{-1} - c_{01}\mathbf{C}_{\mathrm{i}}\overline{\mathbf{C}^{-1}}\big)^{\mathrm{D}}\mathbf{C}_{\mathrm{i}}, \quad \mathbf{C}_{\mathrm{i}}|_{t=0} = \mathbf{C}_{\mathrm{i}}^{0}, \tag{5}$$

where η is a viscosity; the superimposed dot stands for the material time derivative. In the simplest formulation we set $\eta = const$ (so-called Newtonian viscosity), but some stress-dependent modifications will be considered in the current study as well.

The model is thermodynamically consistent whenever $\eta > 0$. From the current Lagrangian formulation, the objectivity of the material model is obvious.

2.2 Eulerian formulation

In order to formulate the Simo and Miehe model of the Maxwell fluid on the current configuration, we introduce the left elastic tensor of Cauchy-Green type

$$\mathbf{B}_{\mathrm{e}} := \hat{\mathbf{F}}_{\mathrm{e}}\hat{\mathbf{F}}_{\mathrm{e}}^{\mathrm{T}}. \tag{6}$$

The Kirchhoff stress $\mathbf{S}$ is computed through

$$\mathbf{S} = 2\rho_{\mathrm{R}}\frac{\partial\psi(\mathbf{B}_{\mathrm{e}})}{\partial\mathbf{B}_{\mathrm{e}}}\mathbf{B}_{\mathrm{e}}. \tag{7}$$

In case of the Mooney-Rivlin potential we have

$$\mathbf{S} = \mathbf{S}^{\mathrm{D}} = c_{10}(\overline{\mathbf{B}_{\mathrm{e}}})^{\mathrm{D}} - c_{01}(\overline{\mathbf{B}_{\mathrm{e}}^{-1}})^{\mathrm{D}}. \tag{8}$$

The Lie derivative (also known as the contravariant Oldroyd derivative) of $\mathbf{B}_{\mathrm{e}}$ is given by

$$\mathfrak{L}_v(\mathbf{B}_{\mathrm{e}}) := \dot{\mathbf{B}}_{\mathrm{e}} - \mathbf{L}\mathbf{B}_{\mathrm{e}} - \mathbf{B}_{\mathrm{e}}\mathbf{L}^{\mathrm{T}}. \tag{9}$$

Here, as before, the superimposed dot stands for the material time rate, $\mathbf{L} := \dot{\mathbf{F}}\mathbf{F}^{-1}$. The flow rule and the initial condition are given by

$$-\mathfrak{L}_v(\mathbf{B}_{\mathrm{e}})\mathbf{B}_{\mathrm{e}}^{-1} = \frac{1}{\eta}\mathbf{S}^{\mathrm{D}} = \frac{1}{\eta}(c_{10}\overline{\mathbf{B}_{\mathrm{e}}} - c_{01}\overline{\mathbf{B}_{\mathrm{e}}^{-1}})^{\mathrm{D}}, \quad \mathbf{B}_{\mathrm{e}}|_{t=0} = \mathbf{B}_{\mathrm{e}}^{0}. \tag{10}$$

Note that all the quantities used in this subsection are invariant under isochoric change of the reference configuration. In that sense, the current formulation is purely Eulerian. Mathematically, this means that the model is w-invariant (cf. [24]), which is a certain type of symmetry. In constructing numerical algorithms we will pay attention to this symmetry property.

3 MODELS WITH A STRESS-DEPENDENT VISCOSITY

3.1 Stress-dependence "from outside"

Let us consider a model of Zener body (also known as a generalized viscoelastic body) with the rheological model shown in Figure 1 (left). The model comprises a hyperelastic spring H and a Maxwell body M; the structure formula of the model is $H|M$ where the vertical line $|$ stands for connection in parallel. By $\mathbf{S}_H$ and $\mathbf{S}_M$ denote the Kirchhoff stresses in the Hooke and Maxwell bodies, respectively. According to the iso-strain assumption, both bodies are subjected to the same strain. Using the Coleman-Noll procedure one obtains for the overall Kirchhoff stress

$$\mathbf{S} = \mathbf{S}_H + \mathbf{S}_M. \tag{11}$$

To be definite, for the hyperelastic spring H we assume the Mooney-Rivlin behaviour. Thus,

$$\mathbf{S}_H = \mathbf{S}_H^{\mathrm{D}} = c_{10}^{(H)}(\overline{\mathbf{B}})^{\mathrm{D}} - c_{01}^{(H)}(\overline{\mathbf{B}^{-1}})^{\mathrm{D}}, \quad \text{where} \quad \mathbf{B} := \mathbf{F}\mathbf{F}^{\mathrm{T}}. \tag{12}$$

For the Maxwell fluid we adopt the constitutive equations from Section 2, where the material parameters c_{10} and c_{01} are replaced by $c_{10}^{(M)}$ and $c_{01}^{(M)}$, respectively. Moreover, we assume that the viscosity η is a function of $\mathbf{S}_H$. In other words, the viscosity depends on the stress "from outside" the Maxwell body. To be definite, we will use the following assumption

$$\eta = \eta_0 \exp\big(-\|\mathbf{S}_H\|/S_0\big), \quad \|\mathbf{S}_H\| := \sqrt{\mathbf{S}_H : \mathbf{S}_H}, \tag{13}$$

where $\eta_0 > 0$ and $S_0 > 0$ are material parameters.

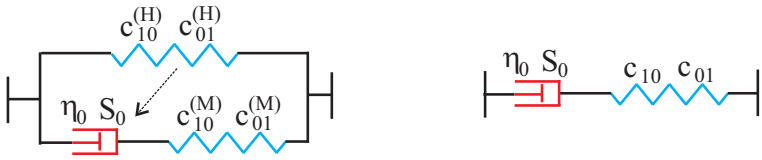

Figure 1: Rheological models and corresponding material parameters. Left: generalized viscoelastic body with stress dependence "from outside" the Maxwell body. Right: Maxwell body with stress dependence "from inside".

3.2 Stress-dependence "from inside"

As an alternative, one may consider the Maxwell body with the viscosity η as a function of the Kirchhoff stress. We consider the evolution equations from Section 2, where

$$\eta = \eta_0 \exp\big(-\|\mathbf{S}\|/S_0\big). \tag{14}$$

Here, again, $\eta_0 > 0$ and $S_0 > 0$ are material parameters. The corresponding rheological interpretation is shown in Figure 1(right).

4 NUMERICAL ALGORITHMS FOR THE BASIC MODEL

Let us consider a generic time step $t_n \mapsto t_{n+1}$, $\Delta t := t_{n+1} - t_n > 0$. In this section we present explicit update formulae for the implicit time integration of the evolution equations (5) or (10).

4.1 Lagrangian algorithm with neo-Hookean potential

First, we consider the constitutive equations from Section 2.1 with $c_{01} = 0$ (neo-Hookean potential). Assume that the current right Cauchy-Green tensor and the previous inelastic right Cauchy-Green tensor are given by ${}^{n+1}\mathbf{C}$ and ${}^{n}\mathbf{C}_\mathrm{i}$. Then the explicit update formula reads (see [15, 21])

$$ {}^{n+1}\mathbf{C}_\mathrm{i} = \overline{{}^{n}\mathbf{C}_\mathrm{i} + \frac{\Delta t\ c_{10}}{\eta} {}^{n+1}\overline{\mathbf{C}}}, \quad {}^{n+1}\tilde{\mathbf{T}} = {}^{n+1}\mathbf{C}^{-1}(c_{10}\overline{{}^{n+1}\mathbf{C}}\ {}^{n+1}\mathbf{C}_\mathrm{i}^{-1})^\mathrm{D}. \tag{15} $$

4.2 Lagrangian algorithm with Mooney-Rivlin potential

For the more general case of the Mooney-Rivlin potential (3), the explicit update formula is summarized in the following computation steps (see [5])

- 1. $\mathbf{A} := \overline{{}^{n+1}\mathbf{C}^{-1/2}}\big({}^{n}\mathbf{C}_\mathrm{i} + \frac{\Delta t}{\eta} c_{10}\overline{{}^{n+1}\mathbf{C}}\big)\overline{{}^{n+1}\mathbf{C}^{-1/2}}$
- 2. $\varepsilon := c_{01}\frac{\Delta t}{\eta}$
- 3. $\varphi_0 := \big(\det \mathbf{A}\big)^{1/3}$
- 4. $\varphi := \varphi_0 - \frac{\mathrm{tr}\mathbf{A}}{3\varphi_0}\varepsilon$
- 5. $\mathbf{X} := 2\mathbf{A}\Big[\Big(\varphi^2\mathbf{1} + 4\varepsilon\mathbf{A}\Big)^{1/2} + \varphi\mathbf{1}\Big]^{-1}$
- 6. ${}^{n+1}\mathbf{C}_\mathrm{i} = \overline{{}^{n+1}\mathbf{C}^{1/2}\ \mathbf{X}\ {}^{n+1}\mathbf{C}^{1/2}}$
- 7. ${}^{n+1}\tilde{\mathbf{T}} = {}^{n+1}\mathbf{C}^{-1}(c_{10}\overline{{}^{n+1}\mathbf{C}}{}^{n+1}\mathbf{C}_\mathrm{i}^{-1} - c_{01}{}^{n+1}\mathbf{C}_\mathrm{i}\overline{{}^{n+1}\mathbf{C}^{-1}})^\mathrm{D}$

In the special case $c_{01} = 0$ the overall procedure reduces to (15).

4.3 Eulerian algorithm with neo-Hookean potential

For the Eulerian formulation summarized in Section 2.2 we have the following iteration-free algorithm. Assume that the current and previous deformation gradients are given by ${}^{n+1}\mathbf{F}$ and ${}^{n}\mathbf{F}$; the previous elastic left Cauchy-Green tensor equals ${}^{n}\mathbf{B}_\mathrm{e}$. First, we define the trial elastic left Cauchy-Green tensor

$$ {}^{n+1}\mathbf{B}_\mathrm{e}^\mathrm{trial} := {}^{n+1}\mathbf{F}\ {}^{n}\mathbf{F}^{-1}\ {}^{n}\mathbf{B}_\mathrm{e}\ {}^{n}\mathbf{F}^{-\mathrm{T}}\ {}^{n+1}\mathbf{F}^\mathrm{T}. $$

Then, dealing with the neo-Hookean potential ($c_{01} = 0$) we have

$$ {}^{n+1}\mathbf{B}_{\mathrm{e}}^{-1} = (\det {}^{n+1}\mathbf{F})^{-2/3}\overline{({}^{n+1}\overline{\mathbf{B}_{\mathrm{e}}^{\mathrm{trial}}})^{-1} + \frac{\Delta t c_{10}}{\eta}\,\mathbf{1}}, \quad {}^{n+1}\mathbf{S} = c_{10}\overline{{}^{n+1}\mathbf{B}_{\mathrm{e}}}^{\mathrm{D}}. \tag{16} $$

In order to avoid redundant computation steps it is more convenient to store ${}^{n}\mathbf{B}_{\mathrm{e}}^{-1}$ instead of ${}^{n}\mathbf{B}_{\mathrm{e}}$. In that case we have $({}^{n+1}\mathbf{B}_{\mathrm{e}}^{\mathrm{trial}})^{-1} := {}^{n+1}\mathbf{F}^{-\mathrm{T}}\,{}^{n}\mathbf{F}^{\mathrm{T}}\,{}^{n}\mathbf{B}_{\mathrm{e}}^{-1}\,{}^{n}\mathbf{F}\,{}^{n+1}\mathbf{F}^{-1}$.

4.4 Eulerian algorithm with Mooney-Rivlin potential

In the more general case of the Mooney-Rivlin potential, the iteration-free algorithm is summarized in the following computation steps (cf. [5]):

- 1. $\tilde{\mathbf{A}} := \overline{({}^{n+1}\mathbf{B}_{\mathrm{e}}^{\mathrm{trial}})^{-1}} + \frac{\Delta t}{\eta} c_{10}\mathbf{1}$
- 2. $\varepsilon := c_{01}\frac{\Delta t}{\eta}$
- 3. $\varphi_0 := \big(\det \tilde{\mathbf{A}}\big)^{1/3}$
- 4. $\varphi := \varphi_0 - \frac{\mathrm{tr}\tilde{\mathbf{A}}}{3\varphi_0}\varepsilon$
- 5. $\overline{{}^{n+1}\mathbf{B}_{\mathrm{e}}^{-1}} = \overline{2\tilde{\mathbf{A}}\Big[\Big(\varphi^2\mathbf{1} + 4\varepsilon\tilde{\mathbf{A}}\Big)^{1/2} + \varphi\mathbf{1}\Big]^{-1}}$
- 6. ${}^{n+1}\mathbf{S} = c_{10}(\overline{{}^{n+1}\mathbf{B}_{\mathrm{e}}})^{\mathrm{D}} - c_{01}(\overline{{}^{n+1}\mathbf{B}_{\mathrm{e}}^{-1}})^{\mathrm{D}}$

In the special case $c_{01} = 0$ this algorithm reduces to (16).

Lagrangian algorithms (cf. Sections 4.1 and 4.2) exactly preserve the w-invariance of the solution; Eulerian versions of the algorithm (cf. Sections 4.3 and 4.4) respect the incremental objectivity restriction. The presented numerical schemes preserve the symmetry of the tensor-valued internal variables ($\mathbf{C}_{\mathrm{i}}$ in the Lagrangian case and $\mathbf{B}_{\mathrm{e}}$ for the Eulerian formulation). Moreover, the incompressibility condition is exactly satisfied which is sufficient to suppress the accumulation of the numerical error [25]. The methods are unconditionally stable and can be used for large time step sizes.

5 NUMERICAL ALGORITHMS FOR THE STRESS-DEPENDENT VISCOSITY

5.1 Numerics: stress-dependence "from outside"

Let us discuss the implementation of the material model with a stress-dependent viscosity described in Section 3.1. As before, consider a typical time step $t_n \mapsto t_{n+1}$. The Kirchhoff stress $\mathbf{S}_H$ pertaining to the Hooke body is evaluated directly, thus giving the current value ${}^{n+1}\mathbf{S}_H$; the current stress ${}^{n+1}\mathbf{S}_M$ related to the Maxwell body is computed using the standard algorithm from Sections 4.2 or 4.4. The only modification is that the viscosity η is formally replaced by the function of already known ${}^{n+1}\mathbf{S}_H$:

$$ {}^{n+1}\eta := \eta_0 \exp\big(-\|{}^{n+1}\mathbf{S}\|/S_0\big). \tag{17} $$

5.2 Numerics: stress-dependence "from inside"

In this subsection we discuss the numerical implementation of the material model from Section 3.2, where the viscosity η depends on the applied stress according to (14). The numerical scheme is a modification of the algorithm, presented in Section 4.2. Assume that ${}^{n+1}\mathbf{C}$ and ${}^{n}\mathbf{C}_{\mathrm{i}}$ are given. Let ${}^{n+1}\tilde{\mathbf{T}}(\eta)$ be a function of η which is obtained by the computational steps 1-7 in Section 4.2. Note that the norm of the Kirchhoff stress can be computed as the following function of the Mandel stress

$$\|\mathbf{S}\| = \sqrt{\mathrm{tr}\big((\mathbf{C}\tilde{\mathbf{T}})^2\big)}. \tag{18}$$

To find the correct value ${}^{n+1}\eta$ one needs to solve the following nonlinear equation

$$g({}^{n+1}\eta) = 0, \quad \text{where} \quad g({}^{n+1}\eta) := {}^{n+1}\eta - \eta_0 \exp\Big(-\sqrt{\mathrm{tr}\big(({}^{n+1}\mathbf{C}\ {}^{n+1}\tilde{\mathbf{T}}({}^{n+1}\eta))^2\big)}/S_0\Big). \tag{19}$$

This equation is solved here using the Newton iteration; the initial approximation for the unknown ${}^{n+1}\eta$ is given by η_0.

Strictly speaking, it is not necessary to solve equation (19) exactly. Simplified solution strategies which provide the solution of (19) with an error $O((\Delta t)^2)$ may be sufficient. Moreover, obviously, the Eulerian algorithm from Section 4.4 can be used as well.

6 DEMONSTRATION PROBLEMS

To test the algorithms we consider a strain-controlled simple shear test. All quantities are non-dimensional in this section. The deformation gradient is given by

$$\mathbf{F}(t) = \mathbf{1} + \mathbf{F}_{12}(t)\mathbf{e}_1 \otimes \mathbf{e}_2, \quad t \in [0, 9], \quad \mathbf{F}_{12}(t) \in [0, 3], \quad |\dot{\mathbf{F}}_{12}(t)| = 1.5. \tag{20}$$

The prescribed dependence of the shear strain on time is shown in Figure 2.

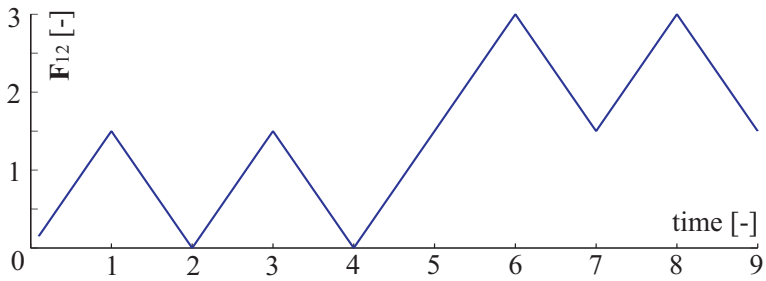

Figure 2: Prescribed dependence of the shear strain on time within the simple shear test.

6.1 Simulations: stress-dependence "from outside"

Here we analyze the algorithm from Section 5.1, which corresponds to the material model described in Section 3.1. The following material constants are used: $c_{10}^{(H)} = 0.5$, $c_{01}^{(H)} = 0.5$, $c_{10}^{(M)} = 1.0$, $c_{01}^{(M)} = 1.0$, $\eta_0 = 0.5$, $S_0 \in \{2, 4, 6, 10\}$.

The simulated shear stress $\mathbf{S}_{12}$ is plotted versus the shear strain $\mathbf{F}_{12}$ in Figure 3. According to the modelling assumption from Section 3.1, the viscosity is a unique function of the instant shear strain. This modelling assumption allows us to capture the changes in the size of the hysteresis loops.

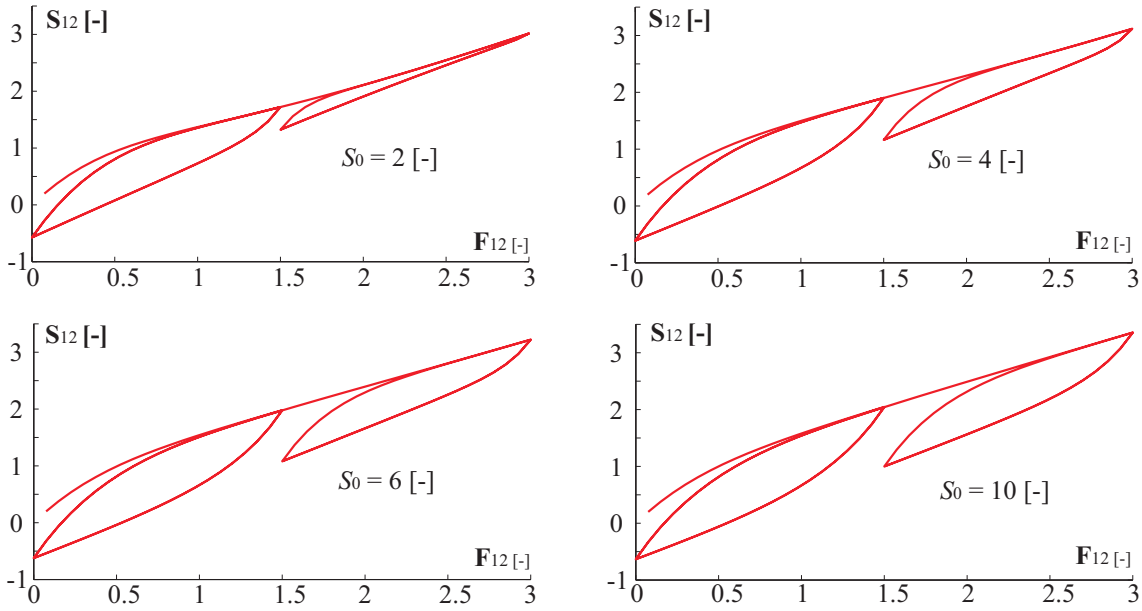

Figure 3: Simulation results for the strain-controlled simple shear test: stress dependence "from outside".

6.2 Simulations: stress-dependence "from inside"

We consider the same simple shear test as in the previous section (cf. Figure 2). The following material constants of the material model from Section 3.2 are used here: $c_{10} = 0.5$, $c_{01} = 0.5$, $\eta_0 = 0.5$, $S_0 \in \{1, 1/2, 1/4, 1/8\}$. Simulation results obtained using the algorithm from Section 5.2 are shown in Figure 4. As can be seen, by adjusting S_0 one can control the shape of the hysteresis loops. In particular, for small values of S_0 the viscosity becomes highly stress dependent. Fast saturation of stress yields material behaviour which resembles elastic-perfectly plastic stress response.

7 DISCUSSION AND CONCLUSION

Substantial progress has been made in construction of efficient and accurate numerical algorithms for the Simo and Miehe (1992) version of the Maxwell fluid. The numerical schemes for constant (Newtonian) viscosity can be generalized to cover various stress-dependent cases in a simple way.

For the Maxwell fluid with a constant viscosity, the corresponding numerical procedure is completely iteration-free. In a more general case of a stress-dependent viscosity, the algorithm can be reduced to a single equation (stress dependence "from inside") or even to an explicit update formula (stress dependence "from outside"). Since various advanced

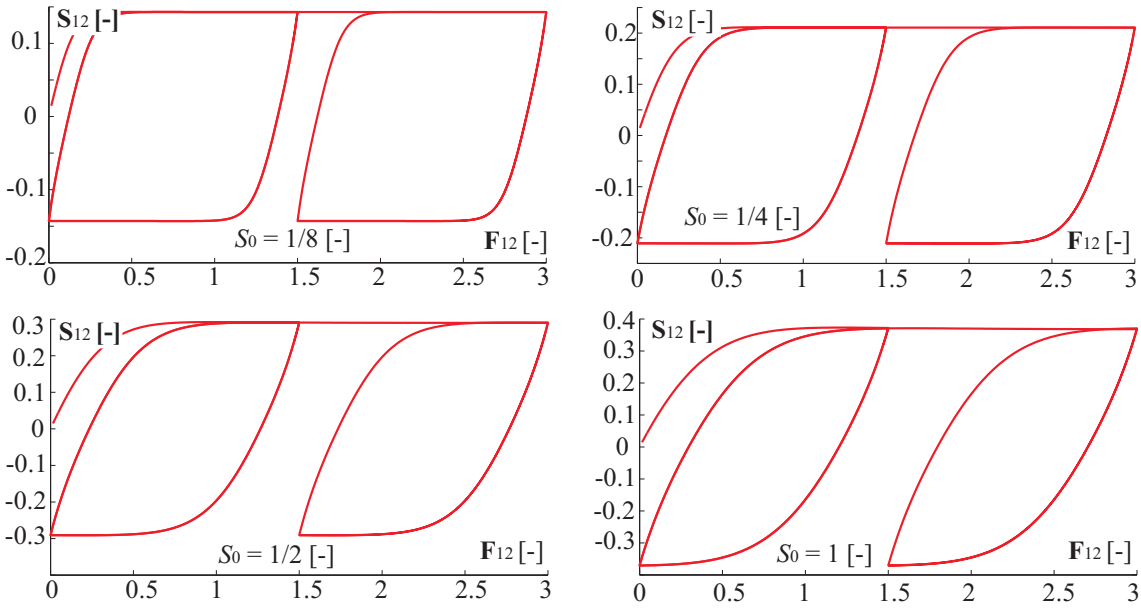

Figure 4: Simulation results for the strain-controlled simple shear test: stress dependence "from inside".

models of visco-elasticity and visco-plasticity comprise the Simo and Miehe (1992) version of the Maxwell fluid, the newly proposed methods can be implemented, thus leading to more robust and efficient numerical procedures.

The research was partially supported by RFBR (grant number 17-08-01020) and by the integration project of SB RAS (project number 0308-2018-0018).

REFERENCES

[1] Simo, J.C. and Miehe, C. Associative coupled thermoplasticity at finite strains: formulation, numerical analysis and implementation. *Computer Methods in Applied Mechanics and Engineering* (1992) **98**:41–104.

[2] Lion, A. A physically based method to represent the thermo-mechanical behaviour of elastomers. *Acta Mechanica* (1997) **123**:1–25.

[3] Shutov, A.V. Seven different ways to model viscoelasticity in a geometrically exact setting. *Proceedings of the 7th European Congress on Computational Methods in Applied Sciences and Engineering* (2016) **1**:1959–1970.

[4] Reese, R. and Govindjee, S. A theory of finite viscoelasticity and numerical aspects. *International Journal of Solids and Structures* (1998) **35**:3455–3482.

[5] Shutov, A.V. Efficient time stepping for the multiplicative Maxwell fluid including the Mooney-Rivlin hyperelasticity. *International Journal for Numerical Methods in Engineering* (2017) **113**:1851–1869.

[6] Simo, J.C. Algorithms for static and dynamic multiplicative plasticity that preserve the classical return mapping schemes of the infinitesimal theory. *Computer Methods in Applied Mechanics and Engineering* (1992) **99**:61–112.

[7] Hartmann, S. *Finite-Elemente Berechnung inelastischer Kontinua. Interpretation als Algebro-Differentialgleichungssysteme*. Habilitation thesis, Kassel, 2003.

[8] Helm, D. Stress computation in finite thermoviscoplasticity. *International Journal of Plasticity* (2006) **22**:1699–1721.

[9] Shutov, A.V. and Kreißig, R. Application of a coordinate-free tensor formalism to the numerical implementation of a material model. *ZAMM* (2008) **88**:888–909.

[10] Vladimirov, I., Pietryga, M. and Reese, S. On the modelling of non-linear kinematic hardening at finite strains with application to springback – Comparison of time integration algorithms. *International Journal for Numerical Methods in Engineering* (2008) **75**:1–28.

[11] Hasanpour, K., Ziaei-Rad, S. and Mahzoon, M. A large deformation framework for compressible viscoelastic materials: Constitutive equations and finite element implementation. *International Journal of Plasticity* (2009) **25**:1154–1176.

[12] Holmes, D.W. and Loughran, J.G. Numerical aspects associated with the implementation of a finite strain, elasto-viscoelastic-viscoplastic constitutive theory in principal stretches. *International Journal for Numerical Methods in Engineering* (2010) **83**:366–402.

[13] Rauchs, G. Finite element implementation including sensitivity analysis of a simple finite strain viscoelastic constitutive law. *Computers and Structures* (2010) **88**:825–836.

[14] Lejeunes, S., Boukamel, A. and Méo, S. Finite element implementation of nearly-incompressible rheological models based on multiplicative decompositions. *Computers and Structures* (2011) **89**:411–421.

[15] Shutov, A.V., Landgraf, R. and Ihlemann, J. An explicit solution for implicit time stepping in multiplicative finite strain viscoelasticity. *Computer Methods in Applied Mechanics and Engineering* (2013) **256**:213–225.

[16] Landgraf, R., Shutov A.V. and Ihlemann, J. Efficient time integration in multiplicative inelasticity. *Proc. Appl. Math. Mech.* (2015) **15**:325–326.

[17] Johlitz, M., Dippel, B. and Lion, A. Dissipative heating of elastomers: a new modelling approach based on finite and coupled thermomechanics. *Continuum Mechanics and Thermodynamics* (2016) **28**(4):1111–1125.

[18] Ghobadi, E., Sivanesapillai, R., Musialak, J. and Steeb, H. Modeling based characterization of thermorheological properties of polyurethane ESTANE. *International Journal of Polymer Science* (2016) **2016** http://dx.doi.org/10.1155/2016/7514974

[19] Silbermann, C.B., Shutov, A.V. and Ihlemann, J. On operator split technique for the time integration within finite strain viscoplasticity in explicit FEM. *Proc. Appl. Math. Mech.* (2014) **14**:355–356.

[20] Shutov, A.V., Silbermann, C.B., Ihlemann, J. Ductile damage model for metal forming simulations including refined description of void nucleation. *International Journal of Plasticity* (2015) **71**:195-217.

[21] Shutov, A.V. Efficient implicit integration for finite-strain viscoplasticity with a nested multiplicative split. *Computer Methods in Applied Mechanics and Engineering* (2016) **306**:151–174.

[22] Shutov, A.V., Larichkin A.Yu. and Shutov, V.A. Modelling of cyclic creep in the finite strain range using a nested split of the deformation gradient. *ZAMM* (2017) **97**:1083–1099.

[23] Schüler, T., Jänicke, R. and Steeb, H. Nonlinear modeling and computational homogenization of asphalt concrete on the basis of XRCT scans. *Construction and Building Materials* (2016) **109**:96–108.

[24] Shutov, A.V. and Ihlemann, J. Analysis of some basic approaches to finite strain elasto-plasticity in view of reference change. *International Journal of Plasticity* (2014) **63**:183–197.

[25] Shutov, A.V. and Kreißig, R. Geometric integrators for multiplicative viscoplasticity: analysis of error accumulation. *Computer Methods in Applied Mechanics and Engineering* (2010) **199**:700–711.